Acta Oceanol. Sin., 2017, Vol. 36, No. 3, P. 1–7
DOI: 10.1007/s13131-016-0882-1
http://www.hyxb.org.cn
E-mail: hyxbe@263.net

An oceanic eddy statistical comparison using multiple observational data in the Kuroshio Extension region

JI Jinlin[1, 2, 3], DONG Changming[1, 3, 4], ZHANG Biao[1, 2, 3*], LIU Yu[1, 2, 3]

[1] School of Marine Sciences, Nanjing University of Information Science and Technology, Nanjing 210044, China

[2] Jiangsu Engineering Technology Research Center of Marine Environment Detection, Nanjing 210044, China

[3] Oceanic Modeling and Observation Laboratory, Nanjing University of Information Science and Technology, Nanjing 210044, China

[4] Department of Atmospheric and Oceanic Sciences, University of California, Los Angeles 90095, USA

Received 3 February 2016; accepted 14 March 2016

Abstract

Eddy characteristics derived from different data resources are compared: sea surface temperature (SST), sea surface height anomaly (SSHA) and surface drifter trajectories. The comparison suggests that the eddy statistical characteristics are different using different variables to delineate eddies, but they show the similar trend. Based on the comparison, abnormal eddies with warm (cold) cores but counter-clockwise (clockwise) rotation are found in the Kuroshio Extension region.

Key words: oceanic eddy, eddy characteristics, Kuroshio Extension region

Citation: Ji Jinlin, Dong Changming, Zhang Biao, Liu Yu. 2017. An oceanic eddy statistical comparison using multiple observational data in the Kuroshio Extension region. Acta Oceanologica Sinica, 36(3): 1–7, doi: 10.1007/s13131-016-0882-1

1 Introduction

Oceanic eddies have been found to play an indispensible role in marine biological and chemical processes (e.g., Vaillancourt et al., 2003; Johnson and McTaggart, 2010; Gruber et al., 2011), and the transport and distribution of heat, salt and energy (Stammer, 1998; Stammer et al., 2001; Roemmich and Gilson, 2001; Jia et al., 2005, 2011; Chen et al., 2012a, b; Volkov et al., 2008; Chelton et al., 2007, 2011; Wang et al., 2012; Bishop et al., 2013; Dong et al., 2014; Zhang et al., 2014). The Kuroshio Extension (KE) region, from Japan eastward to the mid-Pacific, is a band with large eddy kinetic energy (EKE) in the northern Pacific Ocean (Fig. 1) (Qiu and Chen, 2011; Liu et al., 2012; Zhang et al., 2013). Numerous coherent eddies have been detected using altimetry-measured sea surface height anomalies (SSHA) (Ichikawa and Imawaki, 1994; Itoh and Yasuda, 2010; Ji et al., 2016), satellite sea surface temperature (SST) data (Dong et al., 2011a), and drifter trajectories from the global drifter program (GDP) (Dong et al., 2011b).

Itoh and Yasuda (2010) analyzed the characteristics of eddies detected using the SSHA from 1992 to 2008 in the KE region using the Okubo-Weiss (OW) method. Ji et al. [①] employed an automated eddy detection scheme based on eddy geometry to collect eddies and investigate the eddy generation mechanisms in the region. Dong et al. (2011a) detected and analyzed eddies using 9 km SST data for the years 2006–2009, and found more anticyclonic (cyclonic) eddies to the north (south) of the Kuroshio path. Dong et al. (2011b) analyzed an eddy data set for the KE region they derived from the global drifter project (GDP) sea surface drifter trajectories. These studies used different observational data and the question is what the difference among the eddy characteristics revealed by the three data. Motivated by the question, the present study analyzes the eddy data sets from three types of data: SSHA, SST and GDP drifter trajectories (one of coauthors Dong is the leading author for a global SSHA eddy dataset (Dong et al., 2014), also the leading author of two papers on the KE eddies listed above), and readily makes quantitative comparison of the eddy characteristics derived from the three eddy datasets.

The remainder of this paper is organized as follows: Section 2 describes the data and the methodology used in the paper. Section 3 presents the comparison among different eddy data sets from different observational data sources. Section 4 is the summary.

2 Observational data and methodology

2.1 *Observational data*

The following data are used in this study: altimetry SSHA, SST, and GDP drifter trajectories. An automatic eddy detection

Foundation item: The National Natural Science Foundation of China under contract Nos 41476022, 41490643 and 41476158; the Jiangsu Province Science Foundation for Youths under contract No. BK20150897; the Startup Foundation for Introducing Talent of Nanjing University of Information Science and Technology under contract Nos 2013r121 and 2014r072; the National Basic Research Program (973 Program) of China under contract No. 2014CB745000; the National Program on Global Change and Air-Sea Interaction under contract Nos GASI-03-IPOVAI-05 and GASI-IPOVAI-04; the State Key Laboratory of Tropical Oceanography South China Sea Institute of Oceanology Chinese Academy of Sciences under contract No. LTO1407.

*Corresponding author, E-mail: zhangbiao@nuist.edu.cn

[①]Ji Jinlin, Dong Changming, Zhang Biao, et al. Oceanic eddy characteristics and generation mechanisms in the Kuroshio Extension region. (submitted)

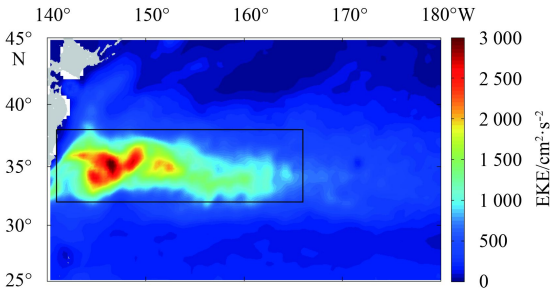

Fig. 1. Spatial distribution of averaged eddy kinetic energy (EKE) with 90-d high pass filter over the period of January 1993 to December 2012. The geostrophic abnormal currents are derived from AVISO SSHA data through geostrophic currents formulae.

scheme based on eddy geometry is employed.

2.1.1 *Altimetry SSHA*

The altimeter products were produced and distributed by archiving, validation and interpretation of satellite oceanographic (AVISO) (http://www.aviso.altimetry.fr/), as part of the SSHLTO ground processing segment. The SSHA data have a spatial resolution of (1/3)° × (1/3)° and a 7-d temporal sampling over the period from October 1992 to August 2013. We focus on the period of January 2006 to December 2011 over the KE region (25°–45°N, 140°–180°E).

2.1.2 *Sea surface temperature*

The SST data are used for the eddy detection, and the detected eddies are compared with those from the SSHA data. The SST data used by Dong et al. (2011a) to derive their eddy data set were downloaded from remote sensing systems (RSS). The product is a daily-sampled merged one with a spatial resolution of 9 km. The data period is between 2006 and 2011.

2.1.3 *Global drifter program (GDP) drifter trajectories*

Sea surface drifter trajectory data are used for the eddy detection, and the detected eddies are compared with those from the SSHA data. The drifter trajectory data are available from the global drifter program website (http://www.aoml.noaa.gov/phod/dac/dacdata.html). The drifters were deployed at a depth of 15 m following near-surface currents. The trajectory data were recorded every 6 h.

2.2 *Methods*

2.2.1 *Eddy detection from SSHA and SST*

In this study, we use an eddy-detection algorithm based on eddy vector geometry proposed by Nencioli et al. (2010). This algorithm has been successfully applied to researching eddies in many different regions, e.g., the lee side of Lanai Island, Hawaii (Dong et al., 2009), the southern California Bight (Dong et al., 2012), subtropical North Pacific Ocean (Liu et al., 2012), leeward of the Madeira Islands (Couvelard et al., 2012), the Balearic Sea (Amores et al., 2013), the Alboran Sea (Peliz et al., 2013), the global ocean (Dong et al., 2014) and the South China Sea (Lin et al., 2015). The eddy detection scheme is briefly introduced below (see Nencioli et al. (2010) for more details). First, four constraints on the geometry of velocity vectors are defined to determine the eddy center.

(1) Along an east-west (EW) section, the v' component of the velocity must reverse in sign across the eddy center, and its magnitude must increase away from the center.

(2) Along a north-south (NS) section, the u' component of the velocity must reverse in sign across the eddy center and its magnitude must increase away from the center. In addition, the sense of rotation for both u' and v' should be the same.

(3) The eddy center is defined as a minimum velocity around the region which extends up to a certain grid point.

(4) The directions of two neighboring velocity vectors around the eddy center must change with a constant sense of rotation and lay within the same or two adjacent quadrants.

For the SSHA data, where u' and v' are the geostrophic current anomaly calculated from the AVISO SSHA data.

$$u' = -\frac{g}{f}\left(\frac{\partial h'}{\partial y}\right), \tag{1}$$

$$v' = \frac{g}{f}\left(\frac{\partial h'}{\partial x}\right), \tag{2}$$

where h' is the sea surface height anomaly and f is the Coriolis parameter.

For the SST data, where u' and v' are the thermal wind calculated from the RSS SST data. In the Northern Hemisphere:

$$u' = -G_y, \quad v' = G_x, \tag{3}$$

$$u' = G_y, \quad v' = G_x, \tag{4}$$

and in the Southern Hemisphere, where G_y and G_x are the Sobel gradient operator. The functions are as follows:

$$G_y = \begin{bmatrix} +1 & +2 & +1 \\ 0 & 0 & 0 \\ -1 & -2 & -1 \end{bmatrix} * A,$$

$$G_x = \begin{bmatrix} +1 & 0 & -1 \\ +2 & 0 & -2 \\ +1 & 0 & -1 \end{bmatrix} * A, \tag{5}$$

where $*$ is the 2-D convolution operation and A is a matrix about the SST data.

Eddy centers are first defined at the points satisfied by all of the constraints listed above. We then searched the outermost closed streamline around the center. If velocity magnitudes cease to increase in the radial direction, it can be regarded as the eddy boundary. A tracking algorithm is also included in the package. We respectively applied this method to 20 years (1993–2012) of altimetry SSHA-derived geostrophic velocity anomalies and 6 year (2006–2011) of RSS SST-derived thermal wind velocity to obtain the eddy data set used in this study, which contains the location of the eddy center, its lifetime, type, size and the locations of its boundaries. As examples to demonstrate how eddies are identified, Fig. 2 shows a snapshot of detected eddies on August 5, 2009, which had a radius of larger than 50 km, along with the geostrophic current anomaly vector field derived from the SSHA data. Besides, Fig. 3 shows a snapshot of detected eddies on December 11, 2006, which had a radius of larger than 20 km, along with the thermal wind vector field derived from the SST data.

2.2.2 *Eddy detection from drifter trajectories*

Dong et al. (2011b) developed a method to identify loops from trajectories as eddies. On the basis of loops detected, the eddy characteristics are determined, such as the eddy size, eddy

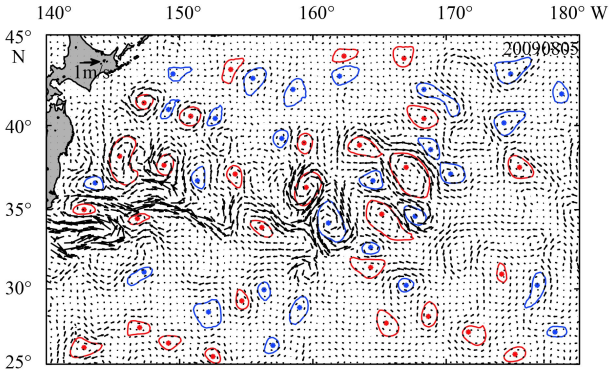

Fig. 2. A snapshot of the geostrophic velocity anomaly field derived from AVISO SSHA data with eddies which have radius larger than 50 km, identified by their center and boundary curves: anticyclonic eddies centers and boundary curves are shown in red, and cyclonic eddies in blue. The snapshot was taken on August.

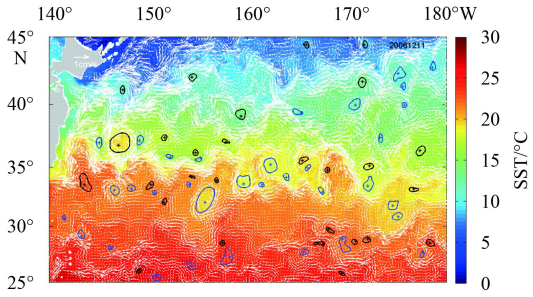

Fig. 3. A snapshot of the velocity of thermal wind derived from RSS SST data with eddies which have radius larger than 20 km, identified by their center and boundary curves: anticyclonic eddies centers and boundary curves are shown in black, and cyclonic eddies in blue. The snapshot was taken on December 11, 2006.

center, and eddy polarity. Two examples are shown in Fig. 4.

3 Results

3.1 *Eddy characteristics comparison*

In order to further examine eddy characteristics, we use the eddy data detected from the SSHA①, the SST (Dong et al., 2011a) and from GDP drifter trajectories (Dong et al., 2011b). We selected the data to be within the same period of 2006–2011. The results of our comparison of the three eddy data sets (SSHA, SST, GDP trajectory) are summarized in Table 1. It should be noted that the three datasets have different temporal sampling and spatial resolutions (Table 1): the SSHA is sampled every 7 d at (1/3)°, the SST daily at 9 km, and the GDP trajectories are sampled every 6 h at random locations. These sampling characteristics can affect the capability to resolve eddies.

During the period, there are 15 097 (14 414) cyclonic (anticyclonic) eddies detected by the SSHA data, and 39 735 (39 652) cyclonic (anticyclonic) eddies detected by the SST data (one snapshot of eddy is considered as one eddy). In addition, there are 1 110 (1 013) cyclonic (anticyclonic) eddies detected by the SSHA data, 5 061 (5 554) cyclonic (anticyclonic) eddies detected by the SST data, and 1 430 (1 684) cyclonic (anticyclonic) eddies detected by drifter trajectories (one-lifetime eddies are considered as one eddy) (Table 1). We find that eddies detected from the GDP trajectories are far fewer in number than those detected from the SST. This is due to the limited availability and spatial sampling of the GDP drifters. In addition, the number of eddies detected from the SST is larger than those detected from the SSHA. This is due to the higher spatial and temporal resolution of the SST. However, although the total numbers of eddies from different sources are different, the numbers of the cyclonic and anticyclonic eddies are statistically equivalent for each data source.

As listed in Table 1, the average radius is the largest for eddies from the SSHA data set (cyclonic: 55.2 km; anticyclonic: 56.7 km), smaller from the GDP trajectories (cyclonic: 36.9 km; anticyclonic: 37.8 km), and smaller still from the SST data set (cyclonic: 41.1 km; anticyclonic: 38.5 km). Although the eddy radius differs across the dataset, they are still close to the first baroclinic deformation radius (≈40 km). As for the average eddy lifetime, the eddies detected from the SSHA have the longest lifetime (cyclonic: 101.5 d; anticyclonic: 105 d), while those from the SST and the GDP are similar to each other but much shorter than those from the SSHA (SST: cyclonic 9.8 d, anticyclonic 9.1 d; GDP trajectories: cyclonic 16.9 d, anticyclonic 16.2 d).

It can be seen that more eddies are detected from SSHA data than those from SST or GDP trajectory data. The reasons are: (1) the SST anomaly is affected by the surface heat flux, oceanic vertical mixing, and an eddy-induced vertical upwelling/downwelling, therefore the SST anomaly induced by an eddy could last much shorter time than that of the SSHA of the eddy; (2) an drifter trapped by an eddy experiences the local rotation effect caused by the eddy, which tends to leave the eddy center, therefore the

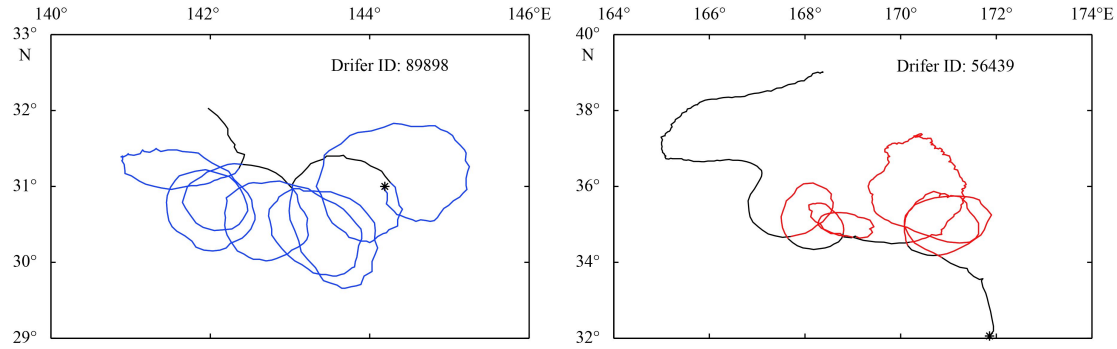

Fig. 4. Examples of loops detected using GDP drifter trajectories. a. Seven counterclockwise loops detected from the trajectory of Drifter 89898, b. six clockwise loops detected from the trajectory of Drifter 56439. Black lines are the drifters' trajectories.

Table 1. Eddy characteristics for the three data sources

Characteristic	SSHA	SST	Drifter trajectories
Data period (year/month)	2006/01–2011/12	2006/01–2011/12	2006/01–2011/12
Temporal resolution	weekly	daily	6 h
Spatial resolution	(1/3)°	9 km	random
Conditions of eddy taken into account	lifetime longer than 4 weeks	lifetime longer than 5 d	eddy radius larger than 5 km
Numbers (cyclone/anticyclone) (1st method)	1 110/1013	5 061/5 554	1 430/1 684
Numbers (cyclone/anticyclone) (2nd method)	15 097/14 414	39 735/39 652	
Radius/km (cyclone/anticyclone)	55.2/56.7	41.1/ 38.5	36.9/37.7
Lifetime/d (cyclone/anticyclone)	101.5/105	9.7/ 9.1	16.9/16.2

drifter can not go with the eddy for a long time, though there are some exceptional cases. Therefore, the primary features of eddies detected from the SSHA, SST and GDP drifters are different, due to the different spatial and temporal sampling frequencies and different physical features.

3.2 *Correlation of eddies from different data sets*

It is interesting to examine how the three sets of observational data present the same eddies. We focus on those eddies that can be collocated in the three data sets during the period of 2006–2011. We identify four subsets: the first includes the eddies collocated using the SSHA and the SST, the second using the SSHA and the GDP, the third using the SST and the GDP, and the fourth using all three (SSHA, SST and GDP). The characteristics we use to classify membership in each subset are lifetime, geographical location and type (cyclonic or anticyclonic). Figure 5 shows an example where the same anticyclonic eddy was detected in all three data sets at the same time. In Fig. 5, the solid line is the GDP trajectory, the vectors represent the AVISO geostrophic current anomaly, and the color is the SST. The figure clearly shows that an eddy can be detected in all three datasets at the same time. Moreover, we followed the eddy shown in Fig. 5, and found that the eddy appears very clearly in all three datasets. We also found that eddies derived from the three data sets correspond better during the mature stage than during youth or old age.

The results for the four subsets are shown in Table 2. From Table 2 it can be seen that 447 (443) cyclonic (anticyclonic) eddies were collocated in the SSHA plus SST data, 796 (943) in the SSHA plus GDP data, 426 (359) in the SST plus GDP data, and 240 (204) in the SSHA plus SST plus GDP data. Note that the number of eddies in the SSHA plus SST set is far lower than that in the SST only dataset (Table 1). The eddies detected by the SST have life-

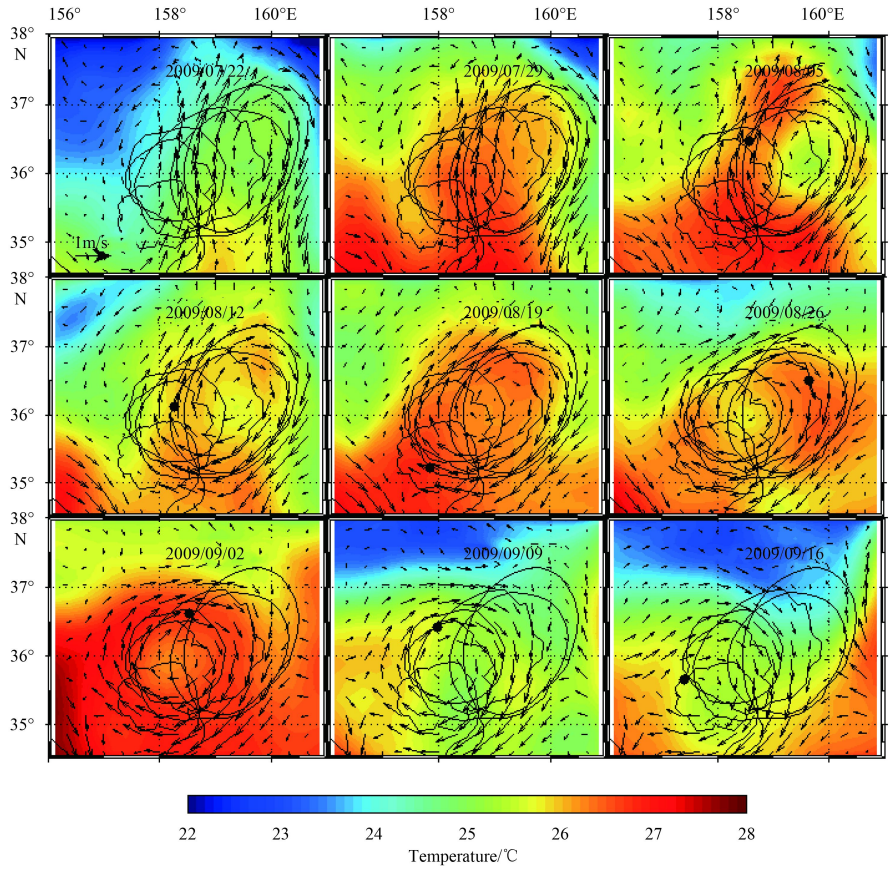

Fig. 5. GDP drifter (No. 18551) and its trajectory (black dots and winding curves) while trapped inside an anticyclonic eddy. The color indicates AVHRR sea surface temperature (SST), vectors are AVISO surface geostrophic velocity anomalies, and the black dots indicate the GDP.

Table 2. Comparison of different eddy datasets detecting the same eddies

Data	Number (cyclone/anticyclone) (1st method)	Radius/km (cyclone/anticyclone)	Lifetime/d (cyclone/anticyclone)
SSHA plus SST	447/443	60.4/59.6 (SSHA) 41.4/38.8 (SST)	102.0/96.9 (SSHA) 11.3/10.1 (SST)
SSHA plus GDP	796/943	60.0/61.7 (SSHA) 36.1/36.0 (GDP)	158.8/161.4(SSHA) 17.8/16.0 (GDP)
SST plus GDP	426/359	45.7/39.4 (SST) 41.6/47.8 (GDP)	15.7/12.2 (SST) 18.3/20.7 (GDP)
SSHA plus SST plus GDP	240/204	64.8/66.4 (SSHA) 46.8/39.2 (SST) 41.5/48.2 (GDP)	186.0/182.9 (SSHA) 16.9/13.3 (SST) 18.2/21.0 (GDP)

times which are far shorter than those detected from the SSHA. Aside from this, we only consider the eddies with lifetimes equal to or longer than 4 weeks when using the SSHA data set, thus within an eddy lifespan detected by the SSHA, the SST data can detect more than one eddy at the same location, which is why the eddy number when both SSHA and SST are used is far lower than when only using SST data. The SSHA plus GDP set has more anticyclonic eddies than cyclonic eddies. This is due to the fact that GDP drifters will remain trapped in anticyclonic eddies for longer than those trapped in cyclonic eddies. Both sub-mesoscale and mesoscale eddies can be detected using GDP data, but only mesoscale eddies can be detected using SSHA data. Therefore, when the same eddies can be detected in both types of data, only the eddies with longer lifetime and larger radius can be identified in the collocated data, which is similar for the SST plus GDP set. Furthermore, Table 2 shows that for both anticyclonic and cyclonic eddies, the lifetime (17.8/16.0 days) of eddies in the SSH Aplus GDP data is longer than that of eddies in the SST only set. This is also true for all of the other GDP collocated sets. The SST plus SSHA set also shows the same characteristic. Finally, for all collocated sets, the eddies have longer lifetime and larger radius than the eddies detected using only one type of data.

3.3 *Eddy generation distribution comparison*

Though three eddy data sets are different in many aspects as revealed in Section 3.1, the common feature on eddy generation distribution is evident. Figure 6 shows the eddy generation distribution against the latitude by the three eddy data sets. They all show most eddies are generated around the Kuroshio path as shown in Fig. 1. The eddy generation time is defined as the moment when the eddy is detected along its track. The common feature shared by the three eddy data sets indicates that the instability associated with the Kuroshio itself is the main reason for the eddy generation.

3.4 *Abnormal eddies*

We have shown that the collocated data can detect the same eddy, but sometimes the collocation identifies opposite type eddies as the same, such as shown in Fig. 7. In this figure we show a cyclonic eddy detected in the SSHA data collocated with an anticyclonic eddy in the SST data. We name such eddies as abnormal eddies. More specifically, the right panel in Fig. 7 shows the geostrophic current anomaly rotating counter clockwise (cyclonic), with the sea surface temperature in the eddy center being warmer than outside the eddy boundary. The left panel shows the opposite case: the geostrophic current anomaly rotating clockwise (anticyclonic), with the sea surface temperature in the eddy center being cooler than outside the eddy boundary. The abnormal eddies are not common phenomenon, most of the abnormal eddies which can not survive longer than 2 weeks. Figure 8 shows the abnormal eddies number distribution against latitudes. There are more cyclonic (anticylonic) eddies with warm (cold) core in south (north) of the Kuroshio axis. The reason is that when the water mass is trapped by a cyclonic (anticyclonic) eddy in the south (north) of the Kuroshio axis, the SST of the water mass is warmer (colder). It is interesting to examine the ver-

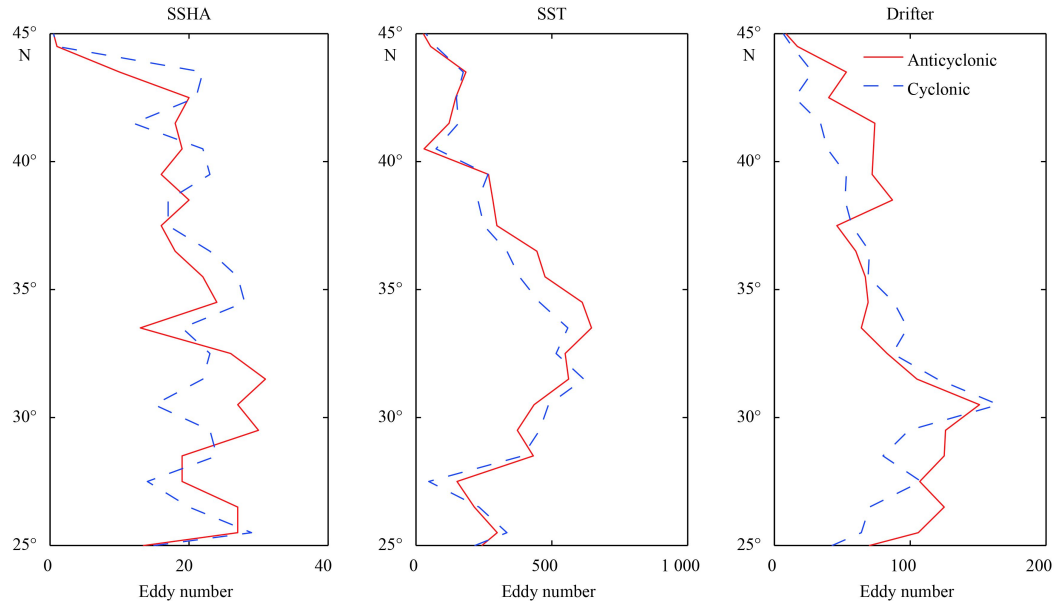

Fig. 6. Numbers of eddy generation at the latitude: (blue solid line) cyclonic and (red thick dashed line) anticyclonic. Left panel is the result of SSHA eddy data set (eddy size larger than 40 km), middle panel is the SST eddy data set (lifetime longer than 5 d) and the right panel is GDP drifter trajectories eddy data base.

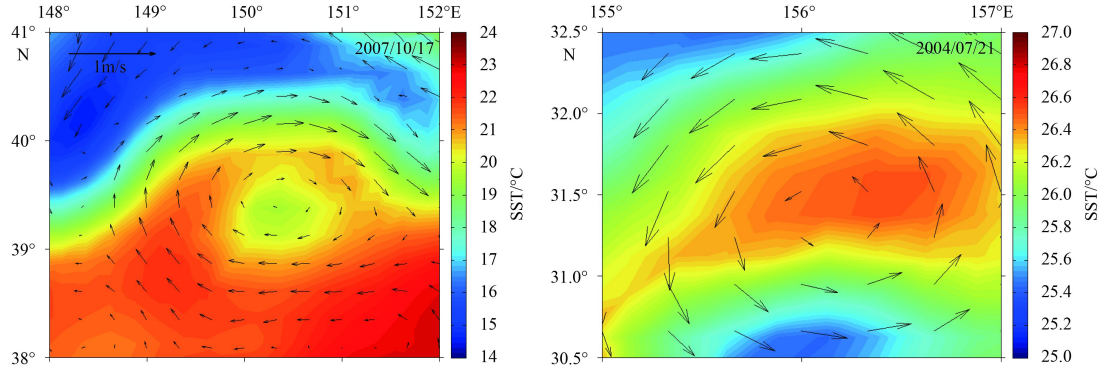

Fig. 7. Two examples of abnormal eddies. The arrows indicate the sea surface anomaly current, and the color is the sea surface temperature. The left panel shows an anticyclonic eddy with lower temperature inside than outside the eddy boundary. The right panel shows the opposite case: a cyclonic eddy with higher temperature inside than outside.

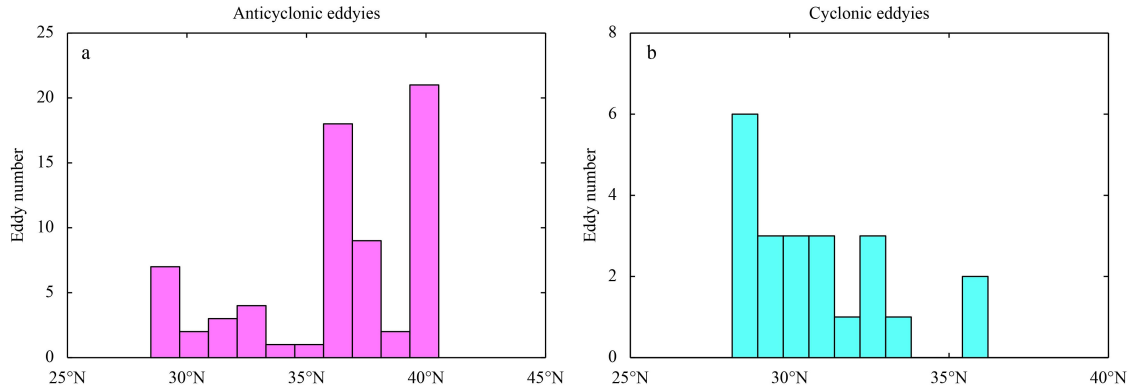

Fig. 8. Abnormal eddies number distribution against latitudes: anticyclonic eddies with cold core (a) and cyclonic eddies with warm core (b).

tical structure to understand how it can exist, but in the present study we do not have a sufficient number of vertical temperature/salinity profiles to examine the abnormal eddies.

4 Summary

On the basis of three previous works by the authors on eddy detection using different data sources: SST, SSHA and drifter trajectories, we examine the three eddy data sets. The comparison analysis shows the eddy numbers detected from the three data sets are significantly different. However, their generation feature in the eddy generation distribution is similar. The comparison also reveals an interesting phenomenon: abnormal eddies (cyclonic eddy with warm core and anticyclonic eddies with cold core) are identified. Their spatial distributions are discussed.

Acknowledgements

We are grateful to AVISO for providing us with the SSHA data, remote sensing systems for providing us with the microwave OI SST data and GDP for providing us with the trajectory data.

References

Amores A, Monserrat S, Marcos M. 2013. Vertical structure and temporal evolution of an anticyclonic eddy in the Balearic Sea (western Mediterranean). J Geophys Res Oceans, 118(4): 2097–2106

Bishop S P, Watts D R, Donohue K A. 2013. Divergent eddy heat fluxes in the Kuroshio extension at 144°–148°E. Part I: mean structure. J Phys Oceanogr, 43(8): 1533–1500

Chelton D B, Schlax M G, Samelson R M, et al. 2007. Global observations of large oceanic eddies. Geophys Res Lett, 34(15): L15606

Chelton D B, Schlax M G, Samelson R M. 2011. Global observations of nonlinear mesoscale eddies. Prog Oceanogr, 91(2): 167–216

Chen Genxin, Gan Jianping, Xie Qiang, et al. 2012a. Eddy heat and salt transports in the South China Sea and their seasonal modulations. J Geophys Res, 117(C5): C05021

Chen Gengxin, Wang Dongxiao, Hou Yijun. 2012b. The features and interannual variability mechanism of mesoscale eddies in the Bay of Bengal. Cont Shelf Res, 47: 178–185

Couvelard X, Caldeira R M A, Araújo I B, et al. 2012. Wind mediated vorticity-generation and eddy-confinement, leeward of the Madeira Island: 2008 numerical case study. Dyn Atmos Oceans, 58: 128–149

Dong Changming, Mavor T, Nencioli F, et al. 2009. An oceanic cyclonic eddy on the lee side of Lanai Island, Hawai'i. J Geophys Res, 114(C10): C10008

Dong Changming, Nencioli F, Liu Yu, et al. 2011a. An automated approach to detect oceanic eddies from satellite remotely sensed sea surface temperature data. IEEE Geosci Remote Sens Lett, 8(6): 1055–1059

Dong Changming, Lin Xiayan, Liu Yu, et al. 2012. Three-dimensional oceanic eddy analysis in the Southern California Bight from a numerical product. J Geophys Res, 117(C7): C00H14

Dong Changming, Liu Yu, Lumpkin R, et al. 2011b. A Scheme to identify loops from trajectories of oceanic surface drifters: an application in the Kuroshio extension region. J Atmos Oceanic Technol, 28(9): 1167–1176

Dong Changming, McWilliams J C, Liu Yu, et al. 2014. Global heat and salt transports by eddy movement. Nat Commun, 5: 3294

Gruber N, Lachkar Z, Frenzel H, et al. 2011. Eddy-induced reduction of biological production in eastern boundary upwelling systems. Nat Geosci, 4(11): 787–792

Ichikawa K, Imawaki S. 1994. Life history of a cyclonic ring detached from the Kuroshio extension as seen by the Geosat altimeter. J Geophys Res, 99(C8): 15953–15966

Itoh S, Yasuda I. 2010. Characteristics of mesoscale eddies in the Kuroshio-Oyashio extension region detected from the distribution of the sea surface height anomaly. J Phys Oceanogr, 40(5): 1018–1034

Jia Yinglai, Calil P, Chassignet E, et al. 2011. Generation of mesoscale eddies in the lee of the Hawaiian Islands. J Geophys Res, 116(C11): C11009

Jia Yinglai, Liu Qinyu, Liu Wei. 2005. Primary study of the mechanism of eddy shedding from the Kuroshio Bend in Luzon strait. J Oceanogr, 61(6): 1017–1027

Johnson G C, McTaggart K E. 2010. Equatorial pacific 13°C water eddies in the eastern subtropical South Pacific Ocean. J Phys Oceanogr, 40(1): 226–236

Lin Xiayan, Dong Changming, Chen Dake, et al. 2015. Three-dimensional properties of mesoscale eddies in the South China Sea based on eddy-resolving model output. Deep-Sea Res: Part I. Oceanogr Res Pap, 99: 46–64

Liu Yu, Dong Changming, Guan Yuping, et al. 2012. Eddy analysis in the subtropical zonal band of the North Pacific Ocean. Deep-Sea Res: Part I. Oceanogr Res Pap, 68: 54–67

Nencioli F, Dong Changming, Dickey T, et al. 2010. A vector geometry-based eddy detection algorithm and its application to a high-resolution numerical model product and high-frequency radar surface velocities in the Southern California Bight. J Atmos Ocean Technol, 27(3): 564–579

Peliz A, Boutov D, Teles-Machado A. 2013. The Alboran Sea mesoscale in a long term high resolution simulation: statistical analysis. Ocean Modell, 72: 32–52

Qiu Bo, Chen Shuiming. 2011. Effect of decadal Kuroshio extension jet and eddy variability on the modification of north pacific intermediate water. J Phys Oceanogr, 41(3): 503–515

Roemmich D, Gilson J. 2001. Eddy transport of heat and thermocline waters in the north pacific: a key to interannual/decadal climate variability?. J Phys Oceanogr, 31(3): 675–688

Stammer D. 1998. On eddy characteristics, eddy transports, and mean flow properties. J Phys Oceanogr, 28(4): 727–739

Stammer D, Böning C, Dieterich C. 2001. The role of variable wind forcing in generating eddy energy in the North Atlantic. Prog Oceanogr, 48(2–3): 289–311

Vaillancourt R D, Marra J, Seki M P, et al. 2003. Impact of a cyclonic eddy on phytoplankton community structure and photosynthetic competency in the subtropical North Pacific Ocean. Deep-Sea Res: Part I. Oceanogr Res Pap, 50(7): 829–847

Volkov D L, Lee T, Fu L L. 2008. Eddy-induced meridional heat transport in the ocean. Geophys Res Lett, 35(20): L20601

Wang Xidong, Li Wei, Qi Yiquan, et al. 2012. Heat, salt and volume transports by eddies in the vicinity of the Luzon Strait. Deep-Sea Res: Part I. Oceanogr Res Pap, 61: 21–33

Zhang Xiao, Jia Yinglai, Shen Hui, et al. 2013. Review on mesoscale eddy studies in the Kuroshio extension region. Climate Change Res Lett, 2(1): 1–8

Zhang Zhiwei, Zhong Yisen, Tian Jiwei, et al. 2014. Estimation of eddy heat transport in the global ocean from Argo data. Acta Oceanologica Sinica, 33(1): 42–47